Intermetallics 49 (2014) 70–80

Contents lists available at ScienceDirect

Intermetallics

journal homepage: www.elsevier.com/locate/intermet

Fabricating Ni–Mn–Ga microtubes by diffusion of Mn and Ga into Ni tubes

Peiqi Zheng [a], Paul Lindquist [b], Bin Yuan [c,*], Peter Müllner [b], David C. Dunand [a]

[a] Department of Materials Science & Engineering, Northwestern University, Evanston, IL 60208, USA
[b] Department of Materials Science & Engineering, Boise State University, Boise, ID 83725, USA
[c] School of Materials Science and Engineering, South China University of Technology, Guangzhou 510640, China

ARTICLE INFO

Article history:
Received 29 May 2013
Received in revised form
16 January 2014
Accepted 18 January 2014
Available online 14 February 2014

Keywords:
A. Shape-memory alloys
C. Deposition
B. Diffusion
G. Shape-memory alloy applications

ABSTRACT

Tubes of the ferromagnetic shape-memory alloy Ni–Mn–Ga of composition near the Ni_2MnGa Heusler phase can be used, alone or combined in structures, in magnetic actuators or magnetic refrigerators. However, fabrication of Ni–Mn–Ga tubes with sub-millimeter diameter by classical cold or hot drawing methods is hampered by the brittleness of the alloy. Here, we demonstrate a new process, where Ni–Mn–Ga tubes are fabricated by interdiffusion of Mn and Ga into drawn, ductile Ni tubes with 500 and 760 μm inner and outer diameters. After interdiffusion and homogenization of Mn and Ga at 1000 °C for 24–36 h, Ni–Mn–Ga tubes with ~300 and ~900 μm inner and outer diameters were obtained with homogeneous radial composition distribution, independently of the diffusion sequences (i.e., Mn and Ga diffused sequentially or simultaneously). Longitudinal composition was uniform over lengths of ~1 mm, but variable over longer length due to incomplete process control. For two of the three diffusion sequences, a sizeable (20–80 μm) region exhibiting Kirkendall pores formed at the outer surface of the tubes. Magnetization values as high as ~60 emu/g were measured, which is comparable to the magnetization of the Ni_2MnGa Heusler phase. X-ray diffraction on the tube with the highest magnetization confirmed the room-temperature structure as cubic austenite.

1. Introduction

The Ni–Mn–Ga ferromagnetic shape memory alloys (FSMA) with composition near the Ni_2MnGa Heusler phase exhibit magnetic superelasticity [1], very large magnetic-field-induced strains (MFIS) [2] and a giant magnetocaloric effect (MCE) [3]; they are thus promising materials for shape-recovery devices, actuators and magnetic refrigeration. Ni–Mn–Ga single crystals show very large MFIS of ~10% [4], but the fabrication of single crystals is time-consuming, expensive and difficult; by contrast, polycrystalline Ni–Mn–Ga alloys with small grain size show negligible MFIS (<0.01%) because grain boundaries inhibit the motion of twin boundaries needed for MFIS. To reduce constraints from grain boundaries, bamboo grain structures were created in foam struts or fibers [5,6]. Recently, Chmielus et al. [7] reported that polycrystalline Ni–Mn–Ga foams with bimodal pore sizes exhibit up to 8.7% MFIS. Dunand and Müllner [8] proposed that large MFIS in polycrystalline Ni–Mn–Ga may be possible when the grain size is comparable to one or more dimensions of the FSMA element. Various sample shapes with high surface to volume ratios, such as films, powders, or fibers with bamboo grains can be used to build Ni–Mn–Ga constructs with different scales and architectures.

Ni–Mn–Ga fibers are difficult to fabricate with sub-millimeter diameter and high aspect ratios, because the brittleness of the alloy prevents cold or hot fiber drawing. Dunand and Müllner [8] proposed that Ni–Mn–Ga fibers could be created by depositing Mn and Ga on the surface of Ni fibers. Ni–Mn–Ga hollow fibers or tubes with sub-millimeter diameter are more difficult to fabricate than solid fibers. Such Ni–Mn–Ga microtubes may be useful for magnetic refrigeration that requires fluid flow through the MCE elements [9], or a stiff and strong MFIS actuators.

In the present study, we demonstrate a new method to create Ni–Mn–Ga microtubes. Commercial-grade Ni microtubes with 760 μm outer diameter and 500 μm inner diameter are coated with Mn by electro-deposition and then filled with liquid Ga. To achieve a homogenous Ni–Mn–Ga composition, Mn and Ga are diffused into the Ni tubes and homogenized at elevated temperature. The

* Corresponding author.
E-mail address: apsheng@scut.edu.cn (B. Yuan).

0966-9795/$ – see front matter © 2014 Elsevier Ltd. All rights reserved.
http://dx.doi.org/10.1016/j.intermet.2014.01.014

advantages of this approach are: (i) Ni microtubes are commercially available as they can be cold-drawn to submillimeter diameters because of the high ductility of pure Ni; (ii) Mn can be electrodeposited on Ni at ambient temperature; (iii) Ga, which is liquid near ambient temperature, can be injected into the capillary of the Ni tube; and (iv) Mn and Ga can be diffused into Ni at high temperatures to form a homogenous Ni–Mn–Ga alloy, as recently demonstrated for films [10]. Further discussion of other related methods are given in Section 4.1.

2. Experimental procedures

Commercially pure nickel microtubes (Nickel 200, 99.6% purity, purchased from SmallParts Inc.) with inside diameter (ID) of 500 μm, outside diameter (OD) of 800 μm and wall thickness of 150 μm, were ultrasonically cleaned in acetone for 15 min. To obtain the correct Ni/Ga and Ni/Mn atomic ratios, the microtubes were chemically etched in an acid solution ($1HNO_3$:2HCl:$2H_2O$) at 60–70 °C for 20 min under ultrasonic agitation. Based on optical measurement of the microtube, the ID remained constant at 500 μm and the OD decreased to 760 μm, corresponding to a 130 μm wall thickness. This wall thickness was chosen so that, after Ga fills completely the Ni tube and diffuses in it, an atomic ratio of Ni/Ga = 2.35 would be achieved, which is close to the composition for off-stoichiometry Ni–Mn–Ga with 10 M martensite and large MFIS [11], $Ni_{50.3\pm0.9}Mn_{28.5\pm0.5}Ga_{21.2\pm0.2}$ (Ni/Ga = 2.37 ± 0.09 and Ni/Mn = 1.77 ± 0.14). The thinned Ni tubes were ultrasonically cleaned in acetone, alcohol and deionized water for 15 min respectively, and dried in air at 80 °C for 30 min. Gallium warmed above its 29 °C melting point was drawn into a syringe, and then injected into the Ni tubes which were filled completely, as determined by letting the Ga overflow from the other end of the tubes during injection. The filled Ni tubes were then crimped closed with pliers.

Manganese was electroplated on the outer surface of the Ni tube from 0.6 M manganese sulfate and 1 M ammonium sulfate aqueous solution [12], with a pH adjusted to 2.8–3.0 with ammonium hydroxide and sulfuric acid. The plating occurred at a current density of 100 mA/cm^2 while rotating the tube at 1 RPM in a beaker with a platinum-coated titanium anode until a thickness of ~64 μm Mn (~50 mg for a length of 40 mm) was reached. This corresponds to an atomic ratio of Ni/Mn = 1.74, which is close to the Ni/Mn = 1.77 ± 0.14 ratio cited earlier. Ni tubes plated with Mn and/or filled with Ga were placed vertically in a tube furnace with titanium getter pieces, then evacuated to 6×10^{-4} Pa, and after heating, back-filled with argon to $1.2 \cdot 10^5$ Pa pressure. The Ni tubes were heat treated at elevated temperature for times sufficient for thermal diffusion and homogenization to occur, and then cooled in furnace.

Three different processing routes were explored to identify the most efficient process sequence to achieve the final composition, as shown schematically in Fig. 1. In Route 1, the Ni tube was first electroplated with Mn, followed by heat treating at 1000 °C for 12 h. After cooling, the Ni–Mn tube was injected with liquid Ga and subjected to a second heat treatment at 1000 °C for 12 h to achieve the Ni–Mn–Ga alloy composition. In Route 2, the Ni tube was first filled with liquid Ga and heat-treated at 1000 °C for 12 h. The Ni–Ga tube was then electroplated with Mn and heat treated at 1000 °C for 24 h to achieve the Ni–Mn–Ga alloy composition. In Route 3, the Ni tube was first electroplated with Mn and filled with liquid Ga, and then heat treated at 1000 °C for 24 h. Each route was carried out on two sets of tubes which are labeled, according to the route used, as 1, 2, 3 and 1*, 2*, 3*, respectively. Every processing parameters was the same, except that Tube 1* was subjected to 24 h (rather than 12 h) for the second heat treatment at 1000 °C. Furthermore, Tubes 1, 2, 3 were sectioned, and one section of each

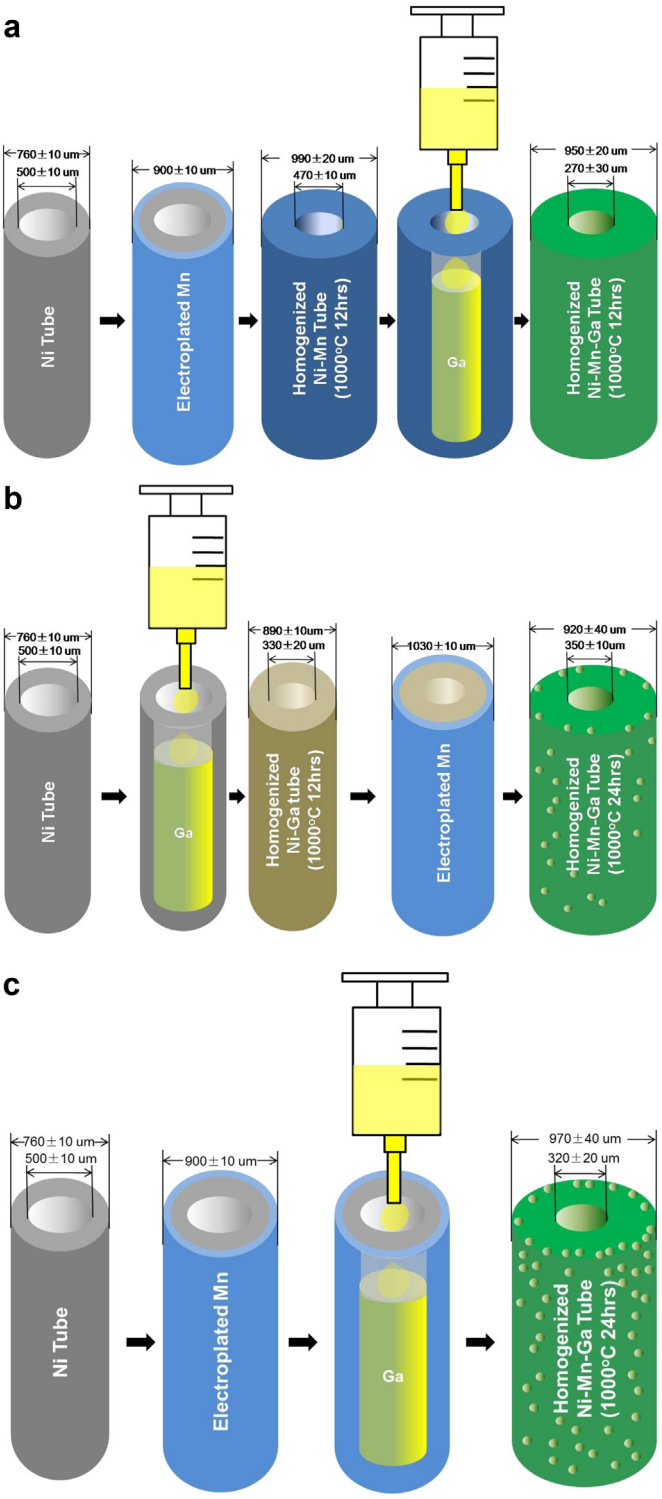

Fig. 1. Schematic of the three processing routes used to create Ni–Mn–Ga tubes, with all dimensions measured experimentally and Kirkendall porosity shown schematically a. Route 1 – Step 1: Ni tube is electroplated with Mn and homogenized at 1000 °C for 12 h; Step 2: The liquid Ga is injected into the homogenized Ni–Mn tube and homogenized at 1000 °C for 12 h. b. Route 2 – Step 1: Ni tube is filled by liquid Ga and homogenized at 1000 °C for 12 h; Step 2: The homogenized Ni–Ga tube is electroplated with Mn and homogenized at 1000 °C for 24 h. c. Route 3 – The Ni tube is electroplated with Mn, filled with liquid Ga, and homogenized in a single step at 1000 °C for 24 h.

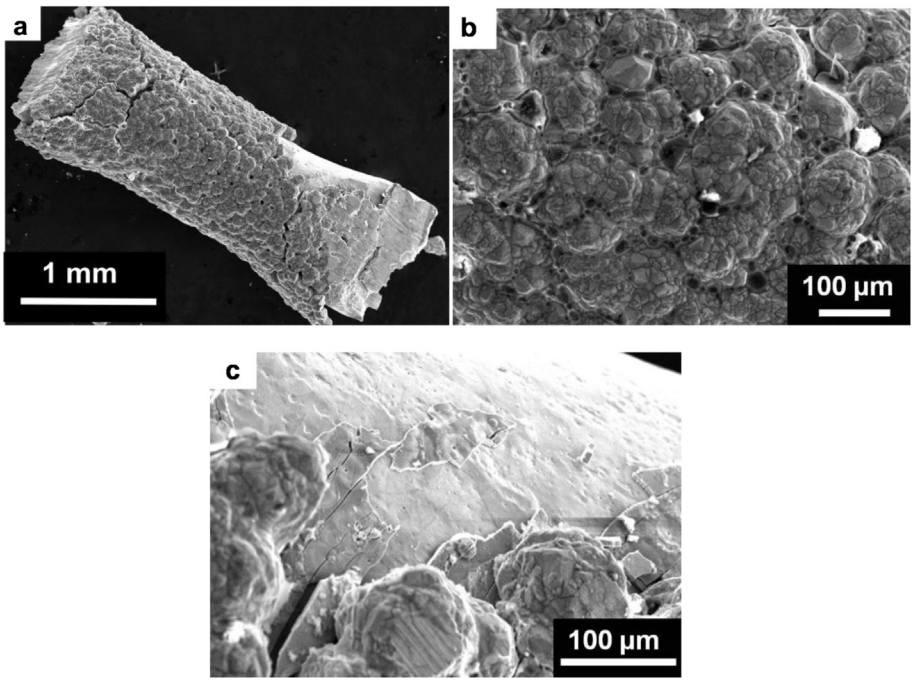

Fig. 2. SEM micrographs of the surface of Tube 1a after Mn plating, showing: a. the Mn-coated region at low magnification; b. the Mn-coated region 1 in a. at higher magnification; c. region 2 in a, where the Mn coating has peeled, revealing the smooth Ni surface.

tube, labeled 1′, 2′, 3′, was aged at 750 °C for 12 h to create the $L2_1$ structure.

For each tube, two separate polished cross-sections, labeled ′ and ″, were imaged with an Olympus optical microscope, and the tube diameters were averaged from four measurements offset by 45°. Cross-sections were imaged by scanning electronic microscopy (SEM, Hitachi S-3400N) with an energy dispersive x-ray detector (EDS, Oxford) for chemical composition analysis carried out along longitudinal and radial directions. The composition of all samples were measured at the same instrument setting (i.e. at constant accelerating voltage, probe current and working distance) calibrated with a Ni–Mn–Ga standard sample whose chemical composition had been measured independently by wet chemical analysis. The line-scans in all composition profiles are unitless and are shifted individually to match quantitative composition point measurements from EDS. They can thus be used to visualize the composition gradients, while the individual points provide quantitative composition information. All average compositions were measured by EDS with area detection over the whole cross-section of the tube.

For each process sequence, the magnetization of the sample, with length ~1 to ~5 mm (and mass of 6–30 mg), was measured in a vibrating sample magnetometer (VSM, DMS Model 10). To detect the martensite phase transformation, the samples were heated and cooled between −60 and 150 °C in the VSM while measuring the change in sample magnetization at a constant magnetic field of 250 Oe. These samples were tested "as processed", described in Route 1 through 3 above. The samples were then heat treated at 750 °C for 12 h at 133.3 Pa. Ar pressure and the magnetic properties of the samples were tested again. For the sample with

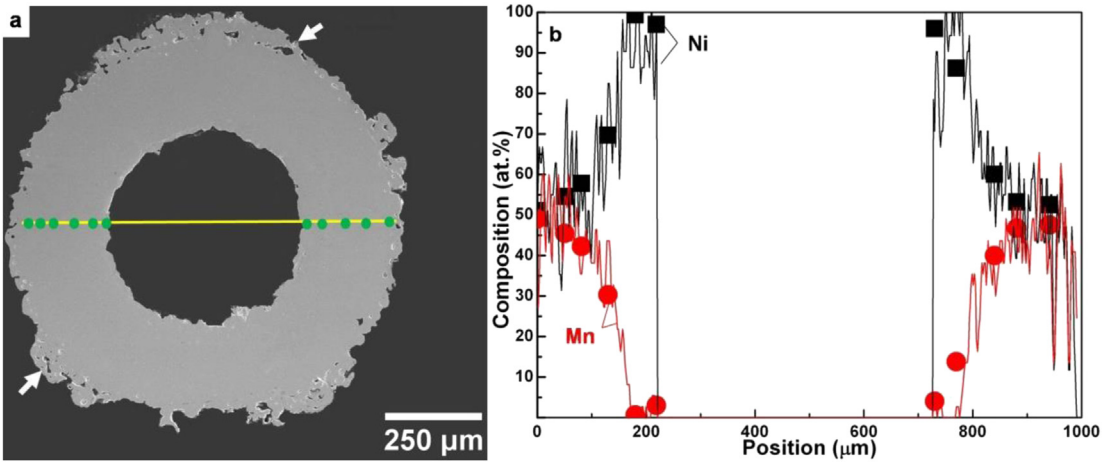

Fig. 3. Tube 1a after Mn plating and annealing (Route 1): a. SEM image of radial cross-section 1a″, with porous outer surface shown with white arrows; b. Plot of Mn and Ni radial composition as line-scan (arbitrary units) and point scan (at.%) along line shown in a.

Table 1
Tube diameters (measured and reference values based on stoichiometric $Ni_{50}Mn_{25}Ga_{25}$) and compositions for all samples.

Route	Sample	Cross section[a]	Average composition (at.%)			Diameters (μm)		Porosity
			Ni	Mn	Ga	ID	OD	
–	Ni	′	100	0	0	500 ± 10	760 ± 10	None
1	Ni–Mn (1a)	′	Not measured			480 ± 10	960 ± 20	~50 μm porous outer layer
		″	64.7	35.3	0	470 ± 10	990 ± 20	
		Ref.	67	33	0	490	890	–
	Ni–Mn–Ga (1b)	′	47.1	29.2	23.7	260 ± 20	930 ± 20	None
		″	52.0	37.5	10.6	270 ± 30	950 ± 20	
		Ref.	50	25	25	230	890	–
2	Ni–Ga (2a)	′	67.7	0	32.3	360 ± 30	820 ± 10	None
		″	56.6	0	43.4	330 ± 20	890 ± 30	
		Ref.	67	0	33	330	850	–
	Ni–Ga–Mn (2b)	′	55.5	22	22.5	320 ± 30	900 ± 20	~20 μm porous outer layer
		″	56.1	25.5	18.4	350 ± 10	920 ± 40	
		Ref.	50	25	25	330	935	–
3	Ni–Mn–Ga (3)	′	47.1	34.9	18.0	340 ± 10	1000 ± 20	~80 μm porous outer layer
		″	47.8	34.6	17.6	320 ± 20	970 ± 40	
		Ref.	50	25	25	320	925	–

[a] Cross-sections 1 and 2 are labeled with ′ and ″ respectively in text.

the highest magnetization, X-ray diffraction (XRD, Bruker D8) was done to determine the structure of the alloy. The X-ray tube was furnished with a copper target run at 40 kV and 40 mA with a 1 mm collimator and a nickel filter. Diffracted intensity was collected with a Bruker Hi–Star area detector. The sample stage was oscillated ±2 mm orthogonal to the X-ray detector plane and the results are a composite of three scans where the samples were rotated between scans.

3. Results

3.1. Route 1 – sequential Mn and Ga interdiffusion

After Mn electroplating, a small piece of the tube was cut with scissors. Fig. 2a and b shows the surface morphology of Sample 1a: The Mn deposit is nodular and has cracks, indicative of brittleness. Mn adhesion to Ni is low, as shown in region 2 of Fig. 2a where the Ni surface of the tube is exposed due to the lack of Mn, also shown in Fig. 2c.

Fig. 3 shows the radial composition distribution for cross-section 1a″ – where the prime and double prime differentiate the two cross-sections studied – after Mn plating and homogenization. The inner diameter (ID) and outer diameter (OD) of this cross-section were about 470 and 990 μm, respectively (measurement for this and other samples are given in Table 1, with error bars). The ID was close to that of the Ni tube (500 μm), while the OD had increased substantially from the original value of 760 μm. The outer surface of the tube displayed a ~50 μm layer that was porous (as shown with white arrows in Fig. 3a), which is most probably due to the Kirkendall effect. Composition profiles depicted in Fig. 3b show gradients along the cross-section 1a″, indicating that Ni–Mn interdiffusion was only partial for the temperature and time (1000 °C and 12 h) used here. From the outer surface of the tube, the Mn content gradually decreased up to a depth of ~100 μm, and then rapidly dropped to a much smaller value. The average composition of cross-section 1a″ was $Ni_{64.7}Mn_{35.3}$, with a Ni/Mn ratio of 1.83, equal to, within error, the desired value of 1.77 ± 0.14.

After Ga injection into the homogenized Ni–Mn cross-section 1a and heat-treatment, the surface of the tube (Fig. 4a) was smoother than after the Mn diffusion (Fig. 2a) but some small cracks still appeared. At higher magnification (Fig. 4b), twins, indicative of a martensite phase, were visible on the tube surface. To confirm the existence of martensite, a cross-section of the Sample 1b after Ga diffusion was polished and etched. As shown in the inset of Fig. 4b, differential interference contrast revealed martensite needles and twins.

Fig. 5a is the cross-section of cross-section 1b″ after sequential Mn and Ga interdiffusion, which shows a single phase without precipitates and an outer surface smoother and more compact than after Mn interdiffusion (Fig. 3a). For cross-section 1b″ (Fig. 5a), the OD and ID were 950 and 270 μm, respectively. In comparison with Fig. 3 where only Mn diffused

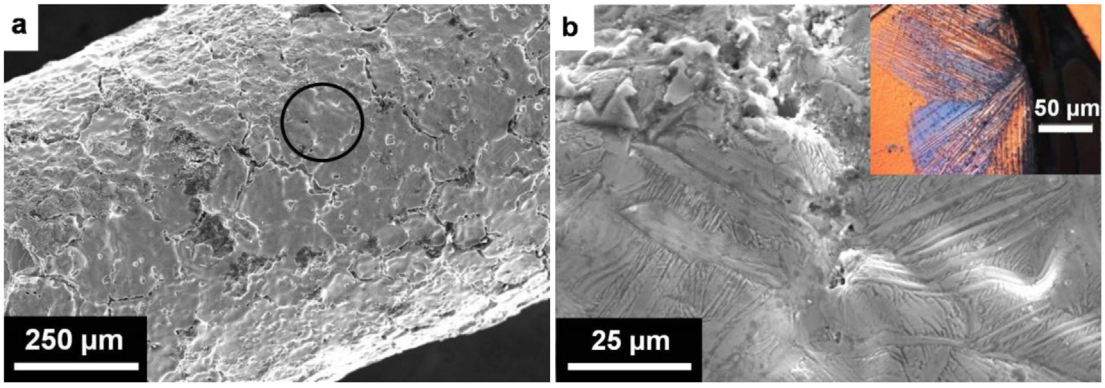

Fig. 4. SEM micrographs of surface of Tube 1b after sequential Mn and Ga interdiffusion (Route 1): a. at low magnification showing surface morphology; b. at higher magnification in circled region in a, showing martensite step traces; inset is optical micrograph of polished and etched section showing martensite laths.

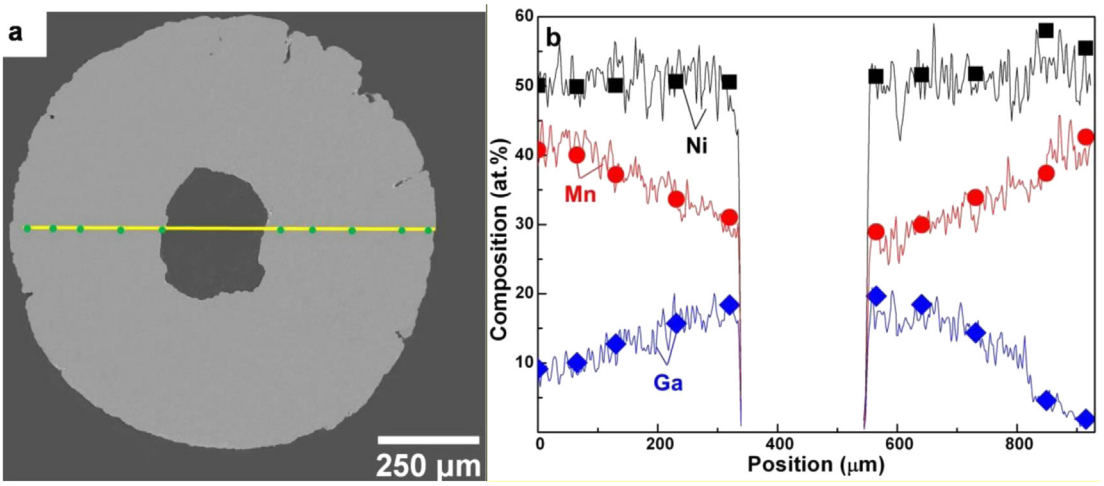

Fig. 5. Tube 1b after sequential Mn and Ga interdiffusion (Route 1): a. SEM image of radial cross-section 1b″, with non-porous outer surface (damage is due to metallographic preparation); b. Plot of Ga, Mn and Ni composition as line-scan (arbitrary units) and point scan (at.%) along line shown in a.

inwards, outward diffusion of Ga does not affect significantly the OD, while the ID is decreased from 470 to 270 μm. Fig. 5b shows Mn and Ga concentration profiles along the cross-section of cross-section 1b″. Comparing Fig. 5b with Fig. 3a shows that the second 12 h annealing further homogenized the Mn within the Ni, yet longer times would be needed to complete Mn and Ga homogenization. The average composition, as measured by EDS area detection over the whole cross section of cross-section 1b″ (Fig. 5a), was $Ni_{52.0}Mn_{37.5}Ga_{10.5}$ (as listed in Table 1). The average composition and sizes of two cross sections of the same tube were measured for all tubes (Table 1). The average composition of cross-section 1b′ was $Ni_{47.1}Mn_{29.2}Ga_{23.7}$, which is different from that of cross-section 1b″ but close to the compositions with large MFIS shown in Fig. 13. The difference may have various origins: (i) variation in the etched tube diameter along its longitudinal direction; (ii) uneven Ga and Mn evaporation at 1000 °C (their partial pressures at 1000 °C are 0.1 and 4.1 Pa, respectively) [13]; (iii) spalling of Mn flakes during heating, due to thermal mismatch stresses and (iv) liquid Ga (and later saturated Ga–Ni) column within the Ni tube breaking up into individual liquid beads as Ga interdiffused (similar to liquid mercury in a thin glass thermometer capillary), leading to regions exposed to Ga for shorter time than others. Concerning the last point, liquid Ga is known to wet pure Ni slightly above room temperature in air [14], a fact confirmed by an experiment where solid Ga was placed on a Ni foil, heated to 45 ± 5 °C and found to wet the Ni foil in the liquid state. Thus, pure Ga is expected to form a continuous liquid film on the inner surface of the Ni tube; however, as Ni diffuses into liquid Ga, its wetting behavior may change.

An extensive processing study, which is beyond the demonstration goal of the present paper, will be needed to determine which of these mechanisms explain the compositional variations between cross-sections.

3.2. Route 2 – sequential Ga and Mn interdiffusion

Fig. 6a and b shows Ni and Ga concentration profiles along a diameter of cross-section 2a″ after Ga injection and homogenization. The composition distribution along the wall thickness was homogeneous within ±5%; also, pores were not present in this Ni–Ga tube, and wall thickness more than doubled from 130 to 280 μm; as listed in Table 1, the ID decreased from 500 to 330 μm and the OD increased from 760 to 890 μm. The composition averaged over the whole cross-sections was $Ni_{56.6}Ga_{43.4}$ for cross-section 2a″, and $Ni_{67.7}Ga_{32.3}$ for cross-section 2a′, as listed in

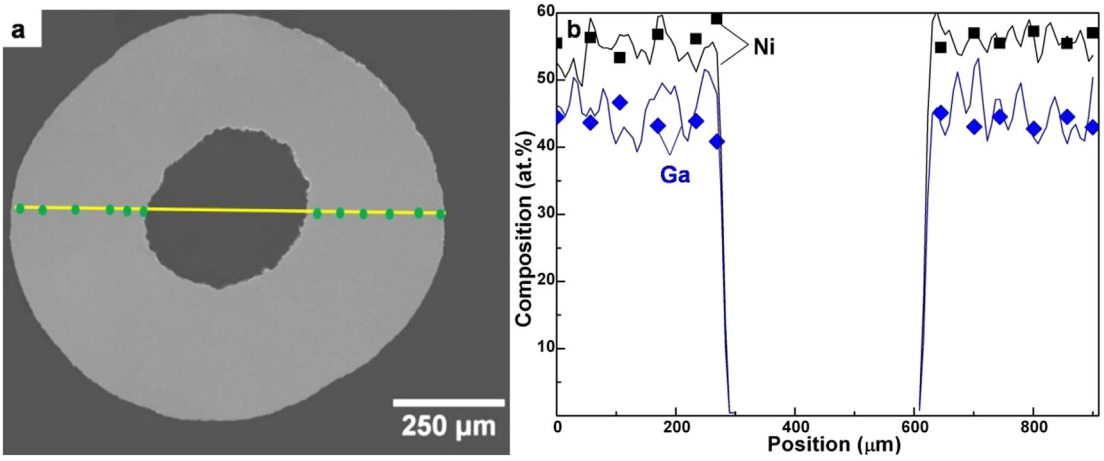

Fig. 6. Tube 2a after Ga injection and annealing (Route 2): a. SEM image of radial cross-section 2a″; b. Plot of Ga and Ni composition as line-scan (arbitrary units) and point scan (at.%) along line shown in a.

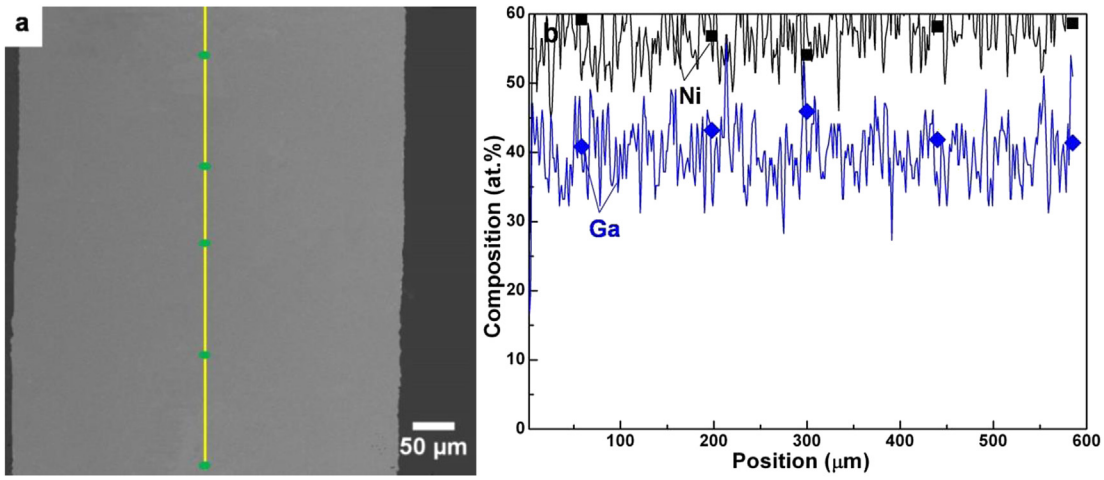

Fig. 7. Tube 2 after Ga injection and annealing (Route 2): a. SEM image of longitudinal cross-section 2a″; b. Plot of Ga and Ni composition as line-scan (arbitrary units) and point scan (at.%) along line shown in a.

Table 1, and this difference may be explained by the same reasons (i), (ii) and (iv) mentioned in the previous section. Thus, a heat-treatment at 1000 °C for 12 h was sufficient for homogeneous interdiffusion of liquid Ga into the solid Ni in the radial direction, but insufficient for homogenization over long distances in the longitudinal direction. For illustration, the longitudinal composition distribution of cross-section 2a″ after Ga interdiffusion, shown in Fig. 7 was homogeneous within ±10% over the 600 μm long area studied.

As the homogenization time for Mn was 24 h (twice 12 h, Fig. 5) in Route 1, the same time for Mn homogenization was adopted for Route 2 to facilitate comparison. Fig. 8 shows the surface morphology of the Ni–Ga–Mn Tube 2b after Mn plating and a subsequent second homogenization. The majority of the surface was covered with micro-pores (region A in Fig. 8a, shown at higher magnification in Fig. 8b), but some regions were nearly pore-free (Fig. 8c). The composition profiles along the diameter are shown in Fig. 9, demonstrating that the composition was radially nearly homogeneous with 10% more Ga and 5% less Mn at the ID than at the OD. The average composition for cross-section 2b″ (Fig. 9a) is $Ni_{56.1}Mn_{25.5}Ga_{18.4}$, which is close to the composition displaying large MFIS (Fig. 13). The OD and ID of this cross-

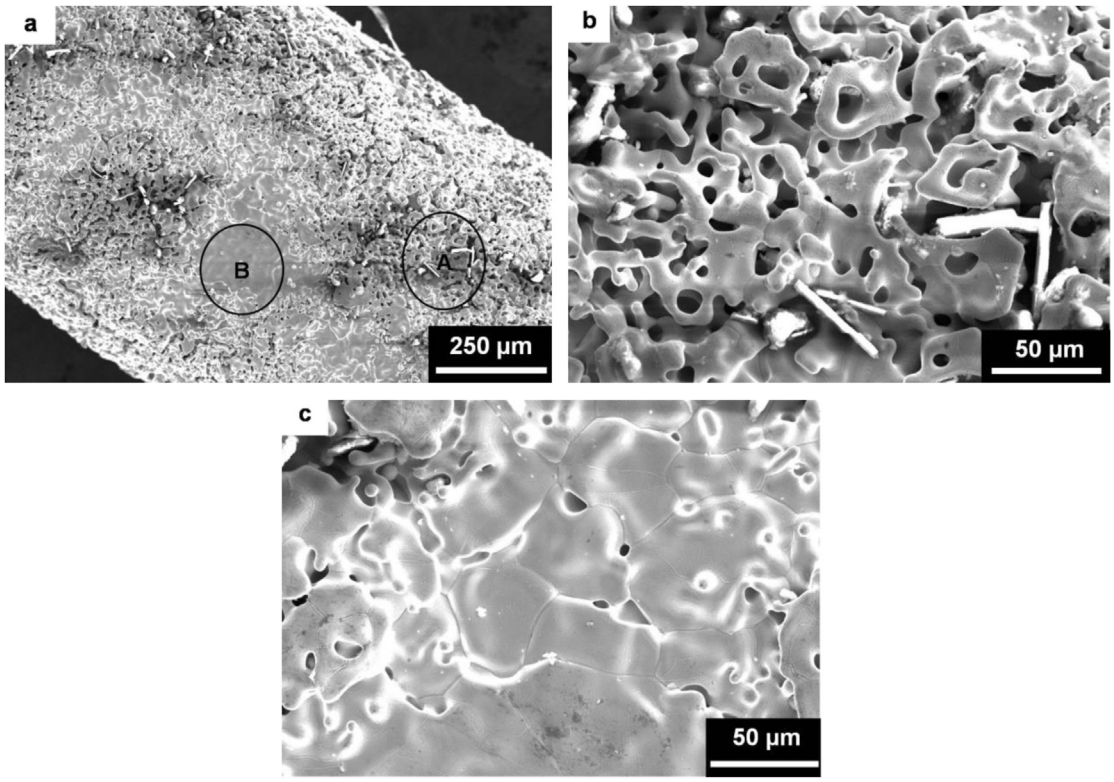

Fig. 8. SEM micrographs of surface of Tube 2b after sequential Ga and Mn interdiffusion (Route 2): a. at low magnification showing surface morphology; b. higher magnification view of region A in a, showing highly porous surface; c. higher magnification view of region B in a showing near dense surface.

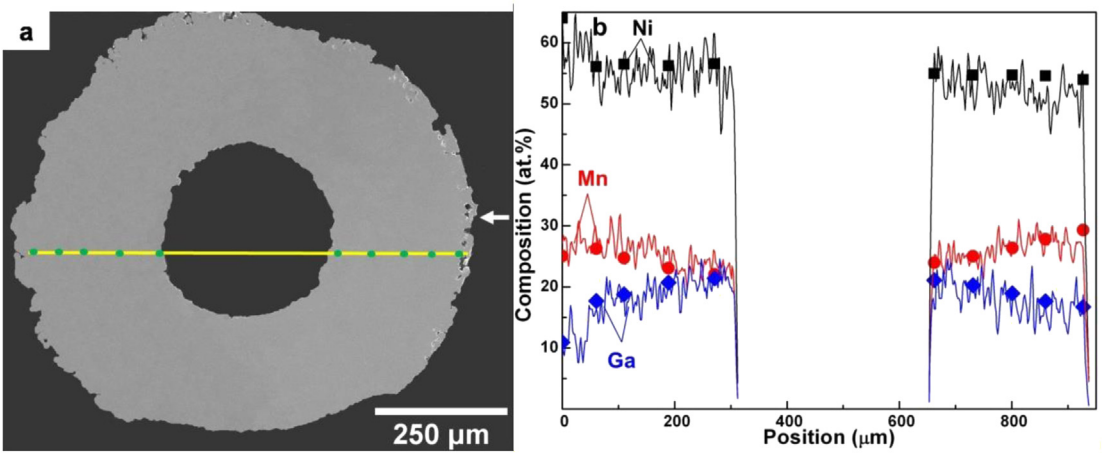

Fig. 9. Tube 2b after sequential Ga and Mn interdiffusion (Route 2): a. SEM image of radial cross-section 2b″; b. Plot of Ga, Mn and Ni composition as line-scan (arbitrary units) and point scan (at.%) along line shown in a.

section were about 920 and 350 μm, respectively, as compared to the original values of 760 and 500 μm, respectively. The microporosity did not extend beyond ~20 μm below the surface (Fig. 9a). The average composition and size results of cross-section 2b′ were different from those of cross-section 2b″, as listed in Table 1. The average composition of cross-section 2b″ is within the range of alloys with large MCE [15].

3.3. Route 3 – simultaneous Mn and Ga interdiffusion

Fig. 10a and b shows the surface morphology of Tube 3 after simultaneous Ga and Mn interdiffusion at 1000 °C for 24 h. The longitudinal composition distribution given in Fig. 11b shows that composition was homogeneous within ±5% over a distance of 650 μm.

Figs. 11a and 12a show cross-sections for cross-section 3″. The microporous layer extended ~80 μm into the tube, as indicated by white arrows in these figures. Decrease in ID and increase in OD were observed, with values reported in Table 1. Fig. 11b shows that the composition is homogeneous over the tube diameter, with an average composition of this overall cross-sectional area (Fig. 12a) being $Ni_{47.1}Mn_{34.6}Ga_{17.6}$, as listed in Table 1. The average composition and size results of cross-section 3″ were very close to those of cross-section 3′ and to the composition displaying large MFIS (Fig. 13).

3.4. Magnetic measurements

Two sets of tubes processed at different times but using the same process sequences, Routes 1–3, were tested for their magnetic properties, as shown in Fig. 14a and b. There was a wide variation from sample to sample and batch to batch in the magnetization of the microtubes. Tube 1* which was homogenized twice as long as Tube 1 had much higher magnetization, indicating that the composition gradients in Tube 1 (Fig. 5b) were reduced by the longer homogenization. For Route 1, the batch-to-batch magnetization variability spanned from 2.5 to 60 emu/g, the latter value being comparable to values reported for Ni–Mn–Ga alloys in this composition range [16]. X-ray diffraction on the sample with the highest magnetization confirmed the room temperature structure as cubic austenite, with $a = 5.798 \pm 0.007$ Å.

The ordering heat-treatment at 750 °C for 12 h increased the magnetization of samples processed via Route 2. The magnetization of Tube 2 whose magnetizations was 2.5 emu/g increased by a factor of 10 after the ordering heat treatment, as shown for Tube 2′ in Fig. 14a. For samples processed via Routes 1 and 3, the ordering treatment had no to little effect on the magnetic properties. This may be explained by their composition difference since magnetic properties are very sensitive to Ni–Mn–Ga's composition. No martensitic phase transformations were observed during heating

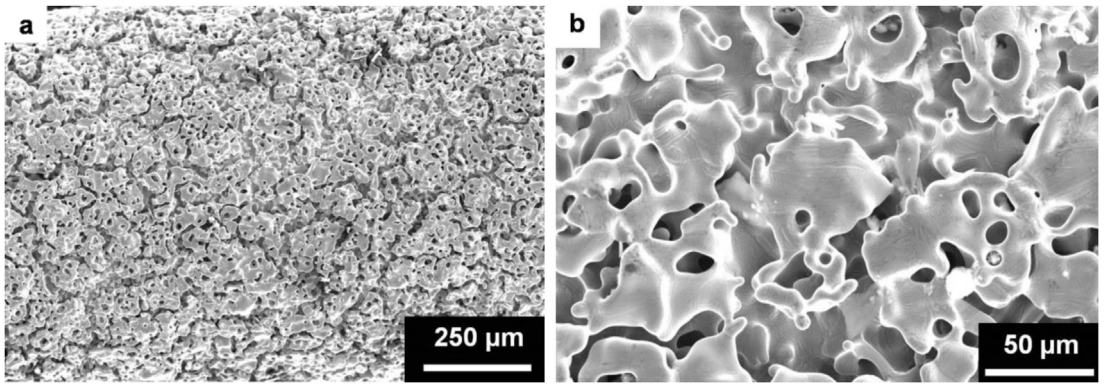

Fig. 10. SEM micrographs of surface of Tube 3 after simultaneous Ga and Mn interdiffusion (Route 3): a. low magnification image showing highly porous surface; b. higher magnification image showing interconnected porosity.

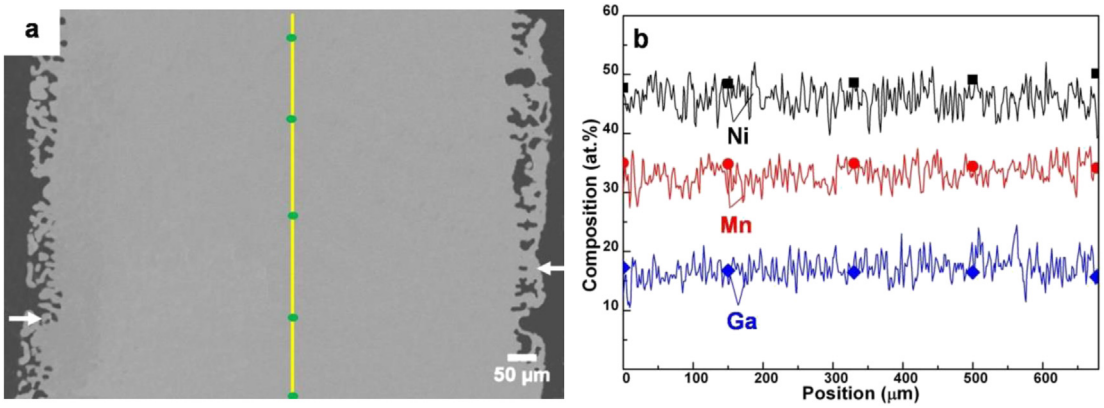

Fig. 11. Tube 3 after simultaneous Ga and Mn interdiffusion (Route 3): a. SEM image of longitudinal cross section 3″; b. Plot of Ga, Mn and Ni composition as line-scan (arbitrary units) and point scan (at.%) along line shown in a.

and cooling between −60 and 150 °C, while measuring the magnetization in a low magnetic field. The Curie temperature varied between 90 and 110 °C.

4. Discussion

4.1. Related processes

The present method for fabrication of Ni–Mn–Ga tubes builds upon a previous study where Ni–Mn–Ga foils were created by interdiffusion of electrodeposited Mn and Ga films onto a ~10 μm thick Ni foil [10] followed by annealing at 800–900 °C for 3–7 h to achieve a homogeneous composition. The concentration gradients equilibrated along the thickness direction but the in-plane composition distribution was inhomogeneous because of the large deposition area (1×1 cm^2). The relative magnetization of the annealed Ni–Mn–Ga film was approximately twice that of the tri-layered as-plated film before homogenization. XRD analysis confirmed the presence of several martensite phases and the austenite phase of Ni–Mn–Ga, which indicates that the magnetic shape memory Heusler alloy Ni–Mn–Ga was formed.

Here, we use a modification of this method, using liquid Ga filled in a tube rather than electrodeposited Ga on a foil, and homogenizing over larger interdiffusion distances. In another prior article [17], Ni–Mn–Ga was fabricated by interdiffusion of Ni–Mn/Ga (solid/liquid) and Ni–Ga/Mn (solid/gas) at high temperatures up to 1000 °C: multiple diffusion couples were studied by annealing an arc-melted $10 \times 10 \times 10$ mm^3 Ni–Mn sample in contact with liquid Ga (or a $10 \times 10 \times 10$ mm^3 Ni–Ga sample in contact with Mn plates) from 800 to 1000 °C for different holding time followed by ice–water quenching. The Ni–Mn/Ga solid–liquid interdiffusion is the same as Route 1 in our study, except for the different source of Ni–Mn and the much larger sample volume leading to inhomogeneous Ni–Mn–Ga formation in Ref. [17]. Besides the different source of Ni–Ga, the Ni–Ga/Mn interdiffusion in Ref. [17] is of solid–gas type, while Route 2 in our study is of solid–solid type. In the present study, we also explore the more complex case where interdiffusion occurs among the three elements simultaneously.

The present results on Ni tubes imply that Ni foams and microlattices [18] consisting of hollow struts with submillimeter diameters could be alloyed with Mn and Ga by the interdiffusion process demonstrated here to achieve Ni–Mn–Ga compositions. In fact, Ni foams with hollow struts have been previously alloyed by the gas phase with Al and/or Cr to create Ni-base superalloy compositions [19]. A similar process has been used to alloy with Al, by the gas phase, a pure Ni structure created by the electroplating LIGA

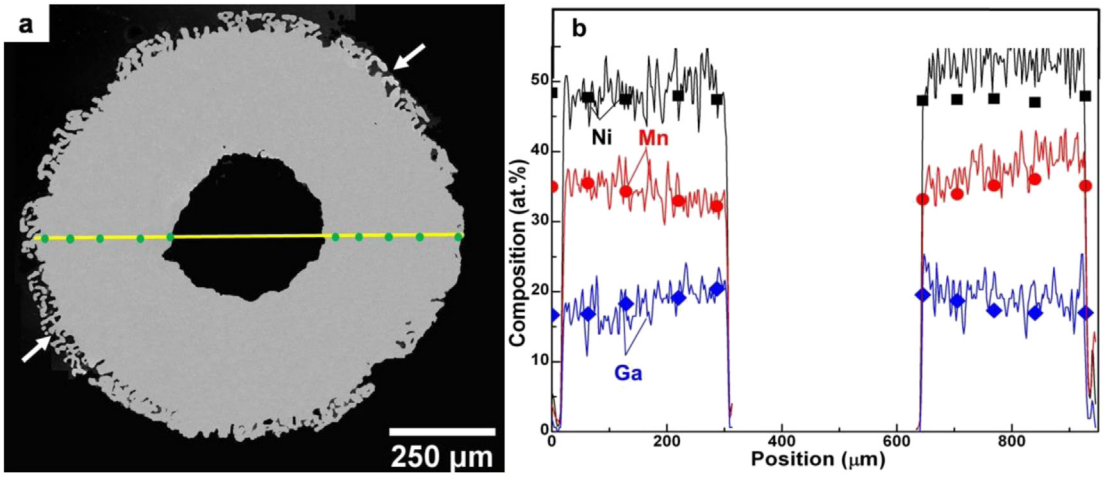

Fig. 12. Tube 3 after simultaneous Ga and Mn interdiffusion (Route 3): a. SEM image of radial cross section 3″, with arrows pointing to surface porosity; b. Plot of Ga, Mn and Ni composition as line-scan (arbitrary units) and point scan (at.%) along line shown in a.

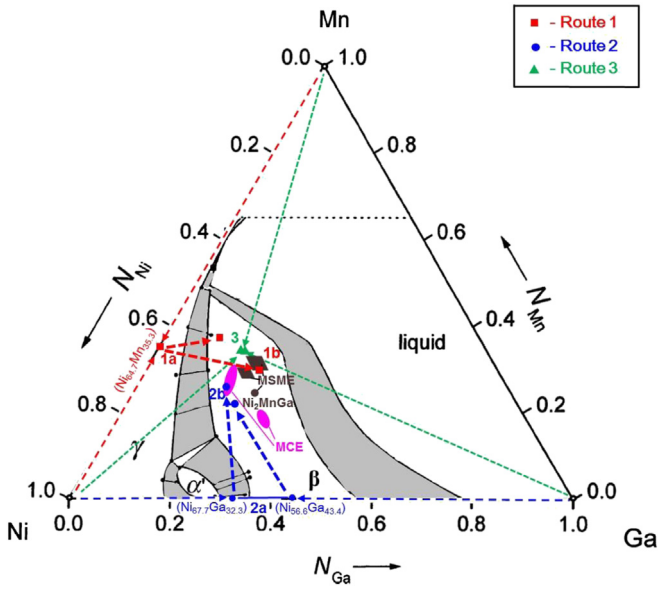

Fig. 13. Isothermal section of the Ni–Mn–Ga ternary phase diagram at 1000 °C reproduced from Ref. [21], with the various routes marked (arrows connect compositions between steps, but do not correspond to the true trajectory of the tubes). Compositions for Ni–Mn–Ga alloy with large MFIS and MCE are from Refs. [11,15].

process [20]; by analogy, the present process could create complex Ni–Mn–Ga MEMS starting from LIGA-deposited nickel structures.

4.2. Interdiffusion

To interpret the phase evolution of the tubes during the interdiffusion process, the isothermal Ni–Mn–Ga phase diagram is reproduced in Fig. 13 [21]. At the processing temperature of 1000 °C, the phase diagram shows the presence of one liquid phase (Ga–Mn with 20–40 at.% Ni) and three solid phases: α′-Ni_3Ga with some Mn substitution, β-Ni(Mn,Ga) and γ-fcc Ni with Ga and Mn in solid solution. The three routes used in the present investigation are marked, with arrows connecting average end-compositions after each step; these arrows do not correspond to composition trajectory of the tubes. Compositions for Ni–Mn–Ga FSMA [11] are also marked on Fig. 13, and are relatively close to the final compositions achieved for each of the routes. Similarly, compositions for Ni–Mn–Ga alloys exhibiting the MCE are shown in Fig. 13, and one tube cross-section processed by Route 2 showed an MCE composition. In this study, the interdiffusion process is complicated by the fact that Ga is liquid at the process temperature, and dissolves large quantities of Ni and Mn. While interrupted diffusion experiments will have to be carried out to identify the intermediate phases created during the interdiffusion process, the following scenarios can be proposed, based on the phase diagram shown in Fig. 13.

For Route 1, the first step is solid-state interdiffusion between Mn and Ni, which occurs according to the published binary phase diagram [22] without formation of intermetallic phases at 1000 °C: the γ-(Ni,Mn) solid solution has the face-centered-cubic crystal structure for a very wide range of Ni, spanning from 6 to 100 at.%. In the second step, when this Ni–Mn solid solution is heated to 1000 °C in the presence of liquid Ga, partial dissolution of the solid is expected to take place until the Ga melt is saturated with Ni and Mn, thus temporarily enlarging the ID of the solid tube. The Ga atoms diffuse outwards into the solid Ni–Mn tube, until the melt composition becomes sufficiently depleted in Ga for its isothermal solidification at 1000 °C. Subsequent interdiffusion between this solidified Ga-rich layer and the solid tube leads to a final single-phase β. The intermediate Ni–Mn and final Ni–Mn–Ga compositions are marked as 1a and 1b, respectively, in Fig. 13.

In the first step of Route 2, where Ni and Ga are initially in contact, the equilibrium phase after full homogenization is close to Ni_2Ga. However, it is again likely that Ni dissolves into the liquid Ga until the melt is saturated at 1000 °C, corresponding to a liquid composition of Ga-35Ni (at.%). The saturated liquid is then at equilibrium with the β-NiGa phase, which has a broad composition of 37–50 at.% Ga at 1000 °C. As interdiffusion proceeds, the Ga content of the liquid drops until it solidifies isothermally at 1000 °C; interdiffusion continues in the solid state, until the equilibrium composition close to Ni_2Ga is reached at 1000 °C: (i) 32.3 at.% Ga for cross-section 2a′, which corresponds to a composition in the β (NiGa) + α′ (Ni_3Ga) two-phase field and (ii) 43.4 at.% Ga for cross-section 2a″, within the β (NiGa) single-phase field [22]. At 25 °C the ID of the Ni–Ga tubes is 330–360 μm. The calculated OD of Ni_2Ga tube from its measured ID value is 849–861 μm, in general agreement with the experimental values of 820 and 890 μm (Table 1). The growth of the OD (as compared to the value for the original Ni tube of 760 μm) during Ga homogenization indicates unbalanced interdiffusion fluxes between Ni and Ga atoms, i.e., more Ga diffuses into the Ni-rich phase than Ni into the Ga-rich phase. All diameter data are listed in Table 1 and calculations are shown in detail in Appendix Table A2.

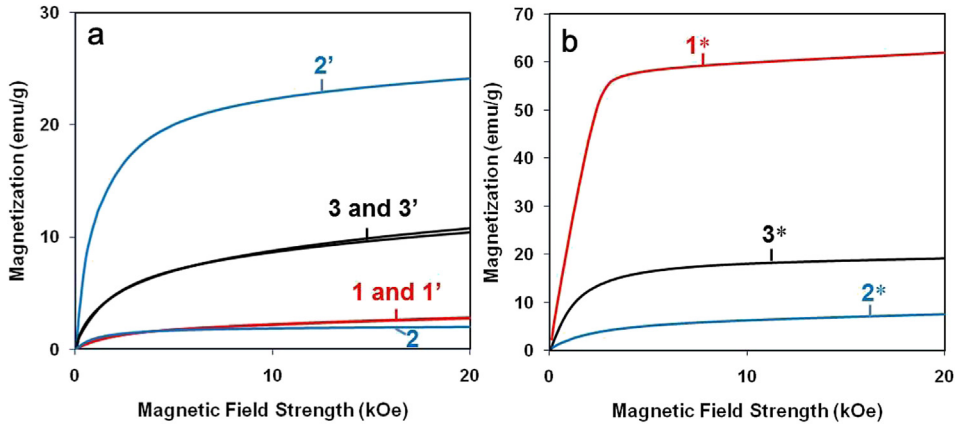

Fig. 14. Magnetization curves of a. as-processed Ni–Mn–Ga tubes from Route 1–3 (labeled 1–3) and the same tubes after chemical ordering at 750 °C for 12 h (labeled 1′–3′); b. another set of as-processed Ni–Mn–Ga tubes from Route 1–3 (labeled 1*–3*), where Tube 1* was homogenized twice as long as Tube 1.

In the second step of Route 2, interdiffusion between the Mn layer and the Ni–Ga tube occurs until the final composition is reached, mostly within the β (Ni_2MnGa) phase field. The measured intermediate Ni–Ga and final Ni–Mn–Ga compositions are marked as 2a and 2b, respectively, in Fig. 13, with cross-section 2b″ being within the MCE composition areas.

For Route 3, it is likely that Ni again dissolves into the liquid Ga within the tube during the early stage as in Route 2, while Mn on the outer surface diffuses inwards as in Route 1. A complex interdiffusion path which cannot be predicted from the equilibrium phase diagram eventually leads to a single phase β (Ni_2MnGa). The measured final Ni–Mn–Ga average compositions are marked in Fig. 13, and are closest to the MSME composition areas.

4.3. Kirkendall porosity

For all three routes, no distortion of the tube is observed, in either the cross-sectional or longitudinal views, despite the large mass fluxes associated with the interdiffusion. The tubes exhibit dense walls, with cross-sections 2b″ and 3″ also showing microporosity concentrated in a relatively thin (20–80 μm) layer on the outer surface of the tube. These pores are most probably due to the Kirkendall effect.

A detailed knowledge of the diffusion path and interdiffusion coefficients may allow prediction of when and where Kirkendall pores may form for each of the routes. These pores are located, for two of the three routes, at the outer surface of the tube, indicating that Mn was diffusing inwards (in the radial direction) more rapidly than Ni (and possibly Ga) did outwards within the tubes. Also, the formation of the central cavity within the core of the tube, which is initially filled with liquid Ga, can be interpreted as the coalescence of Kirkendall vacancies and pores at the solid–liquid interface. This indicates that the outward radial flux of Ga atoms is much faster than the inward Ni and Mn fluxes. The situation is further complicated by the likely evaporation of Mn and Ga during the annealing process, creating another mass transport path for the atoms if they are redeposited at another location in the tube. Detailed measurements using, e.g., thermogravimetry, x-ray 2D and 3D imaging, and backscattered electron image with EDX, in interrupted or in-situ experiments are beyond the scope of the present paper, but will help elucidate the various active mass transport mechanisms during tube homogenization, based on solid diffusion and/or liquid diffusion/convection, solid/liquid dissolution/plating and evaporation/deposition.

4.4. Tube volume expansion

The ID and OD of all tubes in their intermediate stages (either Ni–Mn or Ni–Ga) and final stages (Ni–Mn–Ga) are estimated by calculations based on mass balances, using materials densities and linear thermal expansion coefficients. Various ID and OD combinations can be calculated with the assumption that one of the ID or OD for the Ni (or Ni–Mn or Ni–Ga) tube does not change during alloying, or using as input parameters the measured ID and OD of the Ni–Mn (or Ni–Ga or Ni–Mn–Ga) tubes. The assumption giving the closest match with experiments is used, and the results are listed in Table 1 with detailed calculations given in the Appendix. The assumptions for each route are as follows: Route 1 – the Ni tube ID does not change after Mn diffusion and the Ni–Mn tube OD is unaffected by Ga diffusion; Route 2 – the experimental Ni–Ga tube measured ID is used as input in the calculations, and it is unchanged after Mn diffusion; Route 3 – the Ni–Mn–Ga tube measured ID is used in the calculations.

The stoichiometric $Ni_{50}Mn_{25}Ga_{25}$ composition was chosen as a reference value for experimental results comparison. The calculated diameters based on this stoichiometric composition are compared with the measured diameters in Table 1. In all cases, the calculations are within 20% of the measurements (taking into account error bars), with a systematic bias towards the calculated diameters being smaller than the observed ones. One explanation is that the porous layer near the outside surface of tubes 1a, 2b and 3 results in measured OD being larger than calculated values, where full density was assumed. Other effects noted earlier may also contribute to errors, including evaporation of Mn and Ga during heat-treatments and inhomogeneous interdiffusion along the longitudinal direction.

4.5. Structure and magnetic properties

For sample 1*, the room-temperature structure is single-phase austenite with a saturation magnetization of 60 emu/g (Fig. 14) in agreement with reported data [16]. While the process parameters were designed with the aim to obtain 10 M martensite at room temperature, austenite is stable at room temperature. Various effects may lead to inhomogeneous composition distributions along the fiber axis as discussed above. Strong composition variations may lead to multiphase states with unpredictable magnetic properties. This is reflected in the variability of saturation magnetizations measured for all samples (Fig. 14) indicating that additional research is needed to achieve reproducibility of final composition, which strongly influences martensite structure and martensite transformation temperature.

5. Conclusions

Ni–Mn–Ga microtubes, with ~300 μm inner diameter and ~900 μm outer diameter, were fabricated by radially-inward diffusion at 1000 °C of Mn electrodeposited on a Ni tube outside surface and outward diffusion at 1000 °C of Ga filled in the Ni tube inner cavity. Three routes were explored: in the first two, Mn and Ga are sequentially interdiffused into the Ni tube and, in the third one, interdiffusion of Mn and Ga is simultaneous. In Route 3, the composition is near-homogeneous both in radial and axial direction. For all Routes, average compositions are close to those known to display magnetic-field-induced strains and the magnetocaloric effect. The tube surface morphology, as well as their inside and outside diameters, are affected by the choice of diffusion route, reflecting a complex series of processes including solid-state interdiffusion and possibly solid dissolution in liquid Ga as well as Mn and Ga evaporation. For two of the three sequences studied here, a 50–80 μm porous layer forms at the tube outer surface, which is attributed to Kirkendall porosity. Magnetic properties, which are very sensitive to composition, vary between routes and among samples of a given route. In one instance, the tube with the magnetization of 60 emu/g, comparable to bulk Ni–Mn–Ga alloys processed by casting, was achieved.

Acknowledgments

The authors thank Ms. Nikki Kucza (Boise State University) for assistance with x-ray diffraction experiments. This project was funded by the National Science Foundation through grants DMR-1207282 (Northwestern University) and DMR-1207192 (Boise State University). Authors acknowledge support from the Fundamental Research Funds for the Central Universities (2014ZG0026) and Program for New Century Excellent Talents in University (NCET-12-0201), China.

Appendix. Tube ID and OD calculations

Mass conservation calculations are given in Tables A1–A3 for Routes 1–3, respectively, for intermediate and final steps. In these tables, underlined values are experimental, italic values are assumed (e.g., OD does not change after interdiffusion), bold values are calculated (either using linear thermal expansion or by mass conservation) and the other values are for parameters taken from the following sources. Densities of pure elements at different temperatures are taken from Ref. [23]. Densities of binary alloys are calculated from the densities of pure materials assuming constant atomic volume. The density of the ternary Ni–Mn–Ga at room temperature is from Ref. [24]. The linear coefficient of thermal expansion (CTE) of Ni [25] is used to estimate the Ni tube's diameters change at 1000 °C (1.6%), which determines thickness change of the electroplated Mn layer and the Ga core assuming mass conservation.

Table A1
Calculation of tubes diameters for various steps in Route 1.

Temperature (°C)	Density (g/cm^3)	ID (μm)	OD (μm)
Ni tube			
25	8.90	500	760
1000	8.49	**508**	**772**
Mn-layer on Ni tube			
25	7.43	760	895
1000	6.67	**772**	**919**
Ni_2Mn tube after homogenization			
25	8.33	**490**	**889**
1000	7.76	*508*	**921**
Ga inner core in Ni_2Mn tube			
25	5.91	0	**490**
Ni_2MnGa tube after homogenization			
25	8.13	**228**	*889*

Table A2
Calculation of tubes diameters for various steps in Route 2.

Temperature (°C)	Density (g/cm^3)	ID (μm)	OD (μm)
Ni tube			
25	8.9	500	760
1000	8.49	**508**	**772**
Ga inner core			
25	5.91	0	**500**
1000	5.44	0	**508**
Ni_2Ga tube after homogenization			
25	7.17	330	**849**
		360	**861**
Mn layer on Ni_2Ga tube			
25	7.43	**849**	**984**
Ni_2MnGa tube after homogenization			
25	8.13	*330*	**936**

Table A3
Calculation of tubes diameters for Route 3.

Temperature (°C)	Density (g/cm^3)	ID (μm)	OD (μm)
Ni tube			
25	8.9	500	760
1000	8.49	**508**	**772**
Mn-layer on Ni tube			
25	7.43	760	895
1000	6.67	**772**	**919**
Ga inner core in Ni tube			
25	5.91	0	**500**
1000	5.44	0	**508**
Ni_2MnGa tube after homogenization			
25	8.13	320	**920**

References

[1] Krenke T, Duman E, Acet M, Wassermann EF, Moya X, Manosa L, et al. Phys Rev B 2007;75.
[2] Kostorz G, Mullner P. Z Metallkd 2005;96:703–9.
[3] Gschneidner KA, Pecharsky VK, Tsokol AO. Rep Prog Phys 2005;68:1479–539.
[4] Murray SJ, Marioni MA, Kukla AM, Robinson J, O'Handley RC, Allen SM. J Appl Phys 2000;87:5774–6.
[5] Boonyongmaneerat Y, Chmielus M, Dunand DC, Mullner P. Phys Rev Lett 2007;99.
[6] Scheerbaum N, Heczko O, Liu J, Hinz D, Schultz L, Gutfleisch O. New J Phys 2008;10.
[7] Chmielus M, Zhang XX, Witherspoon C, Dunand DC, Mullner P. Nat Mater 2009;8:863–6.
[8] Dunand DC, Mullner P. Adv Mater 2011;23:216–32.
[9] Bouchard J, Nesreddine H, Galanis N. Int J Heat Mass Tran 2009;52:1223–9.
[10] Gaitzsch U, Drache J, McDonald K, Mullner P, Lindquist P. Thin Solid Films 2012;522:171–4.
[11] Richard M, Feuchtwanger J, Schlagel D, Lograsso T, Allen SM, O'Handley RC. Scr Mater 2006;54:1797–801.
[12] Gong J, Zangari G. J Electrochem Soc 2002;149:C209–17.
[13] Honig RE, Kramer DA. Rca Rev 1969;30:285.
[14] Kamlyabu Hideto, Sakaklbara Akira, Maeda Hironobu, Hida M. Memoirs of the Faculty of Engineering, Okayama University, 23; 1989. pp. 1–8.
[15] Borisenko ID, Koledov VV, Khovailo VV, Shavrov VG. J Magn Magn Mater 2006;300:E486–8.
[16] Jin X, Marioni M, Bono D, Allen SM, O'Handley RC, Hsu TY. J Appl Phys 2002;91:8222–4.
[17] Yang SY, Wang CP, Liu XJ. Intermetallics 2012;25:101–8.
[18] Schaedler TA, Jacobsen AJ, Torrents A, Sorensen AE, Lian J, Greer JR, et al. Science 2011;334:962–5.
[19] Choe H, Dunand DC. Acta Mater 2004;52:1283–95.
[20] Burns DE, Zhang Y, Teutsch M, Bade K, Aktaa J, Hemker KJ. Scr Mater 2012;67:459–62.
[21] Wedel C, Itagaki K. J Phase Equilib 2001;22:324–30.
[22] ASM handbook volume 3: alloy phase diagrams. ASM International; 1992.
[23] Singh RK, Gopalan R. Adv Mat Res 2008;52:57–62.
[24] Webster PJ, Ziebeck KRA, Twon SL, Peak MS. Philos Mag 1984;49:295–310.
[25] Touloukian YS. Thermophysical properties of high temperature solid materials; 1967.